Molecular fingerprints and health risks of home-use incense burning smoke

Kai Song[1,2,#], Rongzhi Tang[3,4,#,*], Jingshun Zhang[5], Zichao Wan[1], Yuan Zhang[6], Kun Hu[1], Yuanzheng Gong[1], Daqi Lv[1], Sihua Lu[1], Yu Tan[7], Ruifeng Zhang[3,4], Ang Li[8], Shuyuan Yan[8], Shichao Yan[8], Baoming Fan[9], Wenfei Zhu[10], Chak K. Chan[3,4], Maosheng Yao[1], Song Guo[1,2,*]

[1] State Key Joint Laboratory of Environmental Simulation and Pollution Control, International Joint Laboratory for Regional Pollution Control, Ministry of Education (IJRC), College of Environmental Sciences and Engineering, Peking University, *Beijing* 100871, China

[2] Collaborative Innovation Center of Atmospheric Environment and Equipment Technology, Nanjing University of Information Science & Technology, *Nanjing* 210044, China

[3] School of Energy and Environment, City University of Hong Kong, *Kowloon* 999077, Hong Kong, China

[4] Shenzhen Research Institue, City University of Hong Kong, *Shenzhen* 518057, China

[5] Shanghai Police College, *Shanghai* 200137, China

[6] School of Earth Science and Engineering, Hebei University of Engineering, *Handan* 056038, China

[7] School of Chemical Engineering and Technology, Sun-Yat-Sen University, *Zhuhai* 519000, China

[8] China Automotive Technology and Research Center (CATARC), *Beijing* 100176, China

[9] TECHSHIP (Beijing) Technology Co., LTD, *Beijing* 100039, China

[10] School of Energy and Power Engineering, University of Shanghai for Science and Technology, *Shanghai* 200093, China

[#] These authors contributed equally to this work.

[*] **Correspondence:** Rongzhi Tang: rongtang@cityu.edu.hk and Song Guo: songguo@pku.edu.cn

28 **Abstract:** The burning of incense for home use is a widespread practice that has been shown to have

29 significant negative impacts on human health and air quality. However, there is a lack of

30 understanding regarding its emission profiles and associated health risks. To address this knowledge

31 gap, we utilized a state-of-the-art thermal desorption comprehensive two-dimensional gas

32 chromatography-mass spectrometer (TD-GC×GC-MS) to (semi-)quantify the emission factors (EFs)

33 of 317 volatile compounds and thoroughly investigate the organic profiles of incense burning smoke

34 across a full-volatility range. Results showed that toluene (70.8 ± 35.7 µg g^{-1}) is the most abundant

35 compound in incensing-burning smoke, followed by benzene, furfural, and phenol. Phenol, toluene,

36 furfural, 2-furanmethanol, benzene, and benzyl alcohol are the main contributors to ozone and

37 secondary organic aerosol (SOA) estimation. Intermediate volatility organic compounds (IVOCs)

38 accounted for 19.2% of the total EFs, but 40.0% of the estimated SOA. Additionally, a novel

39 pixel-based method, combined with aroma analysis, revealed that furfural can act as a key tracer of

40 incense burning, and is responsible for the distinctive flavor of incense smoke. High bioaccumulation

41 potential (BAP) assessment using pixel-based partition coefficient estimation revealed that

42 acenaphthylene, dibenzofuran, and phthalate esters (PAEs) are chemicals of high-risk concern and

43 warrant further control. Our results highlight the critical importance of investigating home-use

44 incense burning and provide new insights into the health impacts of incense burning smoke by novel

45 approaches.

46

1   Introduction

Incense burning is a prevalent custom in many cultures, especially in East and Southeast Asia (Chen et al., 2021). In modern times, incense burning for fragrance has become a frequent practice in households (Manoukian et al., 2013), while functional incense burning, such as mosquito coils, is used for specific purposes. Exposure to incense smoke is linked to adverse health effects like eye irritation, carcinogenicity, genotoxicity, and respiratory system damage (Wong et al., 2020; Yang et al., 2007, 2017). Incense is composed of fragrant materials, aromatic woods, herbs, and adhesive powders, usually available in the form of sticks and coils (Wong et al., 2020; Yadav et al., 2022). Incense burning releases multiple pollutants into the air, including particulate matter (PM), carbon monoxide (CO), volatile organic compounds (VOCs), and intermediate volatility/semi-volatile organic compounds (I/SVOCs) (Wong et al., 2020; Yang et al., 2007; Jetter et al., 2002).

Current studies mainly focus on the hazardous VOC and SVOC homologs released from incense-burning smoke. For instance, Lee et al. investigated 8 carbonyls and 11 VOCs emitted from incense burning and found that the emission factors (EFs) of traditional incense burning were higher than aromatic incense (Lee and Wang, 2004). Lu et al. detected 230 kinds of VOCs from mosquito-repellent incense burning, elucidating that alkanes, esters, aldehydes, ketones, and aromatics are predominant (Lu et al., 2020). Staub et al. measured 6 methoxy phenolics, 10 monoterpenoids, and other 21 kinds of SVOCs in the burning smoke of incense sticks, and identified cedrol as an important odor source (Staub et al., 2011). However, most of the studies have focused on VOC compounds, with less attention given to gaseous organics in the full volatility range (VOC-IVOC-SVOCs). A full-volatility organic characterization may better evaluate the ozone formation potential (OFP) and SOA formation, as I/SVOCs are potentially important precursors of ozone and secondary organic aerosol (SOA) formation (Zhao et al., 2007; Tang et al., 2021; Guo et al., 2014, 2020). Meanwhile, mapping organics from incense smoke helps to evaluate the potential health risks of toxic compounds.

Comprehensive two-dimensional gas chromatography (GC×GC) is a powerful technique dealing with the coelution problem in conventional one-dimensional gas chromatography (1D GC). Pollutants from gasoline exhaust, diesel exhaust, and cooking emissions are well separated and

75 identified (Drozd et al., 2019; Alam et al., 2018; Song et al., 2022a). As much as 50 ~ 98% of the

76 total response in GC×GC chromatograms could be explained (Huo et al., 2021; Song et al., 2022b).

77 Previous work identified 324 compounds from incense smoke by coupling solid-phase

78 microextraction (SPME) with GC×GC, yet chemicals are not quantified (Tran and Marriott, 2007).

79 Thus, a non-targeted and quantitative assessment of incense burning emissions is currently lacking.

80   In this work, two types of incense sticks and three kinds of incense coils were burned in a steel

81 chamber. Gaseous pollutants were trapped by Tenax TA desorption tubes and then analyzed by a

82 thermal desorption comprehensive two-dimensional gas chromatography-mass spectrometer

83 (TD-GC×GC-MS). Pixel-based multiway principal component analysis (MPCA) was utilized to

84 identify markers of incense burning. Risk assessment of pollutants from incense burning emissions

85 was then evaluated by pixel-based approaches and high-risk compounds related to incense burning

86 were assessed.

87 ## 2   Methodology

88 ### 2.1   Sampling and instrumentation

89   Incenses were purchased from the market, including 4 common incense sticks, 2 Thailand

90 incense sticks, 1 mosquito coil, and 2 incense coils (Figure S1). Incenses could also be classified by

91 their material, containing 2 aromatic coils, 4 aromatic sticks, 1 mosquito coil, 1 sandalwood stick,

92 and 1 smokeless sandalwood stick (Figure S1). Incenses were burned in a stainless combustion

93 chamber (1 m^3). After ignition, the burning incense changed from flaming to smoldering. Each kind

94 of incense was burned at least twice. Incenses were weighed before and after combustion.

95 Preconditioned Tenax TA desorption tubes (Gerstel 6 mm 97 OD, 4.5 mm ID glass tube) were

96 utilized to trap organics with a sampling flow of 0.2 L min^{-1}.

97   A comprehensive two-dimensional gas chromatography-quadrupole mass spectrometer

98 (GC×GC-qMS, GC-MS TQ8050, Shimadzu, Japan) coupled with a thermal desorption system (TDS

99 3 C506, Gerstel, Germany) was used for sample analysis. The desorption temperature was 280 °C.

100 The cooled injection system (CIS) with a Tenax TA liner was held at 20 °C and ramped to 320 °C

101 once injecting the gaseous sample into GC columns. The column combination was SH-Rxi-1ms (1st,

102 30 m × 0.25 mm × 0.25 μm) and BPX50 (2nd, 2.5 m × 0.1 mm × 0.1 μm). The modulation period was

103   6s. See Table S1 and elsewhere (Song et al., 2022a) for more information.

2.2   Chemical identification, quantification, and 2D binning

105   A series of standard mixtures (2 μg mL^{-1}, 5 μg mL^{-1}, 10 μg mL^{-1}, 20 μg mL^{-1}, 40 μg mL^{-1} in

106   CH$_2$Cl$_2$) was injected into Tenax TA tubes (2 μL). After purging the solvent with nitrogen gas, the

107   standards were thermally desorbed. The standard mixture contains 26 *n*-alkanes (C7 - C32, CNW

108   Technologies, ANPEL Laboratory Technologies (Shanghai) Inc., China), 16 PAHs, 11 phenolic

109   compounds, 9 alcohols, 4 aldehydes, 8 aromatics, 24 esters, 7 ketones, 5 siloxanes, and 39 other

110   compounds. Gaseous organics are quantified by external calibration curves with most of the R^2

111   between 0.95 and 0.999 (Table S2). Chemicals with the same retention times and mass spectrums

112   were directly qualified and quantified. The unidentified chemicals were qualified by matching their

113   mass spectrum with library spectrums in the National Institute of Standard Technology library (NIST

114   17). Reverse factors of more than 700 were acceptable in this work. As homologs on the

115   two-dimensional chromatogram (contour plot) were eluted with near-equal one-dimensional intervals,

116   chemicals were then qualified by combing the location of the contour plot and the mass spectrums

117   (Song et al., 2023). Compounds without standards were semi-quantified by *n*-alkanes from the same

118   volatility bin (uncertainty 69%) and surrogates from the same chemical class (uncertainty 27%).

119   Instrument detection limits (IDLs) for organics semi-quantified were unknown, as a result, chemicals

120   with negative values calculated by calibration curves were quantified by the volume-to-mass (ng)

121   ratio of the lowest quantification point of standards (Table S2). A total of 317 chemicals were

122   (semi)-quantified, including 10 acids, 34 alcohols, 19 aldehydes, 25 aromatics, 38 esters, 49 ketones,

123   18 *n*-alkanes, 26 nitrogen-containing compounds, and 10 phenols (Table S3).

124   The compounds identified were sliced into two-dimensional bins (2D bins) (Song et al., 2022a).

125   1st retention times are linked to the volatility of species (B8 to B31 with decreasing volatility) while

126   2nd retention times are associated with polarity (P1 to P8 with increasing polarity). Emission factors

127   of compounds in the same 2D bin were aggregated (Table S3).

2.3   Emission factor (EF), ozone formation potential (OFP), and secondary organic aerosol (SOA) estimation

130   The emission factor (EF, μg g^{-1}) was calculated by the following equation:

$$EF = \frac{m\,V}{f\,t\,M} \qquad (1)$$

m is the absolute mass of pollutants (μg) captured by Tenax TA tubes. V is the volume of the steel chamber (1 m^3). The sampling flow and duration of the Tenax TA tube are f (0.0002 m^3 min^{-1}) and t (min), respectively. M is the combustion mass (g) of the incense. The sampling volume of Tenax TA tubes (0.003 ~ 0.01 m^3) was significantly smaller than the total volume of the steel chamber (1 m^3) and the volume change of the chamber could be neglected.

The ozone formation potential (OFP, μg g^{-1}) was calculated using equation (2). EF$_i$ is the emission factor of precursor i (μg g^{-1}) with maximum incremental reactivity (MIR) of MIR_i. The OFP was calculated inside the FOQAT packages developed by Tianshu Chen (https://github.com/tianshu129/foqat). The MIR used in this work can be found in Table S3.

$$OFP = \sum[EF_i] \times MIR_i \qquad (2)$$

Secondary organic aerosol (SOA) was estimated by equation (3).

$$SOA = \sum[EF_i] \times (1 - e^{-k_{OH,i} \times [OH] \times \Delta t}) \times Y_i \quad (3)$$

Where $k_{OH,i}$ and Y_i represent the OH reaction rate and SOA yield of precursor i, respectively (Table S3). The SOA yields of precursors were from literature (Loza et al., 2014; Harvey and Petrucci, 2015; Tkacik et al., 2012; Shah et al., 2020; McDonald et al., 2018; Chan et al., 2010, 2009; Wu et al., 2017; Li et al., 2016; Matsunaga et al., 2009; Algrim and Ziemann, 2019, 2016; Liu et al., 2018; Charan et al., 2020) or surrogates from n-alkanes in the same volatility bins (Zhao et al., 2017). k_{OH} and Y could be found in Table S3. $[OH] \times \Delta t$ is the OH exposure and was set to be 13 $\times 10^{10}$ molecules cm^{-3}s (24 hours in OH concentration of 1.5 $\times 10^6$ molecules cm^{-3}).

2.4 Pixel-based risk assessments of incense-burning pollutants

Octanol-air partition coefficient (K_{o-a}), air-water partition coefficient (K_{a-w}), and octanol-water partition coefficient (K_{o-w}) were estimated by a linear free-energy relationship (LFER) model (Nabi et al., 2014; Zushi et al., 2019). Partition coefficients of chemicals are associated with their two-dimensional retention times (Song et al., 2022b). Chemicals with high bioaccumulation potential (BAP) are defined as contaminants with partition coefficients of (2 < log K_{o-w} < 11) and (6 < log K_{o-a} < 12). See Zushi et al. (Zushi et al., 2019) for more information. The R source code was obtained from GitHub (https://github.com/Yasuyuki-Zushi).

3 Results and discussions

3.1 Emission profiles of different incense-burning organics

Figure S2 is a typical chromatogram of incense burning emissions, which is also set as the reference chromatogram during the pixel-based analysis. As much as 90.2% of the total percent response could be explained. The ratio is similar to a recent study resolving biomass burning emissions (98%) (Huo et al., 2021). The emission factor (EF) of total organics is 791.8 ± 300.6 μg g^{-1}, consistent with previous work (100 ~ 19100 μg g^{-1}) (Lee and Wang, 2004), and comparable to rice (475.9 ± 61.2 μg g^{-1}), pine (558.6 ± 103.6 μg g^{-1}) and poplar (564.6 ± 124.1 μg g^{-1}) combustions (Zhu et al., 2022), but much lower than coal combustion (6.3 mg g^{-1}) (Huo et al., 2021). The contributions of different chemical categories are displayed in Figure S3. Oxygenated compounds dominate the total EFs, accounting for 48.4%, followed by aromatics (29.8%), *b*-alkanes (5.3%), nitrogen-containing compounds (4.0%), alkenes (4.0%), and *n*-alkanes (2.3%). Unresolved complex mixtures (UCMs) are further separated into aliphatic, cyclic, and oxygenated UCM due to retention times and mass spectrums. The UCM ratio in this work (2.3% in EFs) is comparable to biomass burning (Huo et al., 2021) and diesel exhaust (He et al., 2022) analyzed by GC×GC-MS, and is much smaller than the UCM ratio (>50%) in biomass burning smoke analyzed by 1D GC-MS (Zhu et al., 2022). Ketones are the most abundant oxygenated compounds, accounting for 13.6% of the total EFs, followed by aldehydes (9.7%), esters (8.1%), alcohols (6.9%), phenols (3.6%), and acids (3.1%). The emission profiles are comparable to corncob and wood combustion, which are also dominated by ketones and esters (Huo et al., 2021). However, the abundance of phenol is much lower than in biomass-burning smoke (>15%) (Zhu et al., 2022; Huo et al., 2021), while comparable to coal combustion (5.4%) (Huo et al., 2021).

EFs of selected compounds are listed in Table S4, which were comparable with other incense burning studies (Lee and Wang, 2004; Yang et al., 2007; Manoukian et al., 2016), while the EF of benzene (59.6 ± 43.1 μg g^{-1}) is slightly lower than other studies (188 ~ 1826 μg g^{-1}) (Lee and Wang, 2004; Yang et al., 2007; Manoukian et al., 2016). The Tenax TA liner in the CIS system does not capture benzene at an initial temperature of 20 °C, while it is efficient for the trapping of most I/SVOC compounds. Lower CIS temperature may trap benzene while causing water condensation.

187 As a result, the tailing of benzene on the second column (Figure S2) causes an underestimation of

188 blob integration and results in an underestimation of EF.

189   The top 10 compounds are all VOC compounds (Figure S4), accounting for 35.3% of the total

190 EFs. Toluene (70.8 ± 35.7 µg g^{-1}) is the most abundant compound in incensing-burning smoke,

191 followed by benzene, furfural, phenol, styrene, 2-oxo-propanoic acid methyl ester,

192 3-methyl-2-butanone, ethylbenzene, 1-hydroxy-2-propanone, and benzyl alcohol. Note that VOC

193 compounds discussed here are part of volatile organics captured by Tenax-TA, not the common

194 VOCs detected by SUMMA-GC-MS. The top 5 IVOCs are B17 *b*-alkanes, B16 *b*-alkanes, B18

195 *b*-alkanes, diethyl phthalate, and 1,6-dioxacyclododecane-7,12-dione. The naphthalene (a typical

196 PAH, 2 rings) EF is 3.0 ±1.5 µg g^{-1}, comparable to rice straw combustion (Zhu et al., 2022). SVOCs

197 are all *n*-alkane species and only account for less than 1% of the total EFs.

198   The average VBS distribution of incense burning is displayed in Figure 1, and the

199 volatility-polarity distribution is exhibited in Figure S5. In general, the EF decreases as the volatility

200 decreases, following the trend of VOC-EF (80.8%) > IVOC-EF(19.2%) >> SVOC-EF (<0.1%). The

201 chemical compositions in the VOC-IVOC range are shown in Figure S6. Oxygenated compounds

202 (53.5% of the total VOC EFs) and aromatics (37.6%) are largely detected in the VOC range, while

203 *b*-alkanes, *n*-alkanes, and oxygenated compounds are the main components of IVOC compounds.

204 The average VBS distribution is similar to cooking emissions (Song et al., 2022a) and wood

205 combustion (Stewart et al., 2021), but less volatile than gasoline exhausts (Lu et al., 2018) and more

206 volatile than diesel emissions (Lu et al., 2018). For example, the proportion of chemicals with

207 saturated vapor concentration (C*) more than 10^6 µg m^{-3} (Figure 1 a) is 80.8% (incense burning),

208 80.7% (cooking emissions) (Song et al., 2022a), 77.6% (wood combustion) (Stewart et al., 2021),

209 94.2% (gasoline exhaust) (Lu et al., 2018), and 41.0% (diesel exhaust) (Lu et al., 2018). The polarity

210 of incense burning is dominated by non-polar and intermediate-polarity organics (P1 ~ P5, Figure

211 S5). The volatility-polarity distribution of incense burning is quite similar to cooking emissions

212 (Song et al., 2022a), dominant by VOCs in the volatility range of before B13 and the polarity range

213 of P1 ~ P5.

214   A similar emission pattern but different EFs of different incense-burning emissions are observed.

Similarities among incense burning are more dominant than diversities. First, pixel-based partial least squares-discriminant analysis (PLS-DA) elucidates that there is no systemic difference between different chromatograms of incense burning emission, no matter different incense shapes (Figure S7) or materials (Figure S8). Second, the compositions of different types of incense emissions are indeed quite similar (Figure S9 and Figure S10). Third, the multiway principal component analysis (MPCA) positive loadings are much larger than negative loadings, indicating that the similarities between samples are much more important than the differences (Figure 2).

However, the absolute EFs significantly diverge according to different incense forms ($p = 0.03$, Figure S11) and different materials ($p < 0.01$, Figure S12). Incense made in stick form (incense stick: 893.2 ± 335.6 μg g^{-1}, Thailand incense stick: 877.5 ± 123.8 μg g^{-1}) emits more organics than made in coil form (incense coil: 835.5 ± 306.0 μg g^{-1}). The EF of mosquito coil is the smallest (382.5 ± 175.0 μg g^{-1}). A similar pattern was observed in previous work (Jetter et al., 2002). Concerning the incense materials, we spot that the so-called smokeless sandalwood stick emits more abundant organics (1195.8 ± 83.3 μg g^{-1}) than common sandalwood sticks (633.7 ± 6.6 μg g^{-1}). The emission of smokeless sandalwood sticks is even greater than aromatic sticks (893.2 ± 335.6 μg g^{-1}) and coils (824.8 ± 228.5 μg g^{-1}). Our results demonstrate that although smokeless sandalwood stick is preferred as fewer particulates are generated during the combustion process, the gaseous emissions are enhanced compared to other incenses.

3.2 Contributions of home-use incense burning to ozone and secondary organic aerosols (SOA)

The total OFP is 1513.4 ± 551.0 μg g^{-1} which is 1.91 g O$_3$/g VOC-IVOCs. The OFP enhancement ratio (OFP per mass of precursor) is much smaller than gasoline exhaust (3.53 g O$_3$/g VOCs) (Wang et al., 2013) and evaporation (2.3 ~ 4.9 g O$_3$/g VOC) (Yue et al., 2017), showing that incense burning is less efficient on ozone formation than gasoline-related sources. The lack of IVOC measurements in previous work could also cause an overestimation of the OFP enhancement ratio as IVOCs are less efficient in ozone formation. Toluene, furfural, *p*-xylene, benzyl alcohol, phenol, 2-furanmethanol, *o*-xylene, ethylbenzene, 1-hydroxy-2-propanone, and benzene are top 10 species that contribute most to OFP (Figure S4). Oxygenated compounds take up 48.2% of the total OFP,

243   followed by aromatics (41.0%), and alkenes (6.7%) (Figure S3). VOCs dominate the total OFP,

244   accounting for 92.4% while IVOCs take up 7.6% (Figure 1). Aromandendrene, naphthalene, and

245   α-cedrene are the top 3 IVOC-OFP contributors. The volatility distribution of OFP contribution is

246   comparable to cooking emissions, as VOCs account for 88.8 ~ 99.9% of the total cooking OFP

247   estimation (Song et al., 2022a). Toluene contributes the most OFP in both cooking emissions and

248   incense burning. Short-chain linear aldehydes (pentanal, hexanal, nonanal) originating from the

249   degradation of oils play a more important role in OFP contribution in cooking emissions (Song et al.,

250   2022a), while benzenes, furfural, alcohols, and phenols are non-negligible OFP contributors in

251   incense burning.

252   Figure 1 shows the volatility distribution of estimated SOA estimation, with the top 10

253   contributors displayed in Figure S4. IVOCs contribute 19.2% of the EFs while accounting for 40.0%

254   of the total SOA estimation, highlighting the importance of IVOCs in SOA formation. The

255   contribution of IVOC species to SOA is higher than EFs due to the relatively higher yields and k_{OH},

256   which has already been reported in cooking emissions (Song et al., 2022a; Yu et al., 2022), gasoline

257   exhaust (Zhao et al., 2014), diesel exhaust (Zhao et al., 2015), and biomass burning (Stewart et al.,

258   2021). Oxygenated compounds account for 32.9% of the SOA estimation, followed by aromatics

259   (23.7%), and b-alkanes (11.5%) (Figure S3). Phenol, benzyl alcohol, styrene, toluene, B18 cyclic

260   UCM, aromandendrene, 2-furanmethanol, B17 b-alkanes, benzene, and phenyethyne are the top 10

261   SOA contributors. The incense-burning SOA formation profiles are distinct from cooking emissions

262   (Song et al., 2022a) and biomass burning (Huo et al., 2021). Cooking SOA is largely derived from

263   the oxidation of short-chain acids and aromatics (Song et al., 2022a), while phenols account for more

264   than 65% of the SOA estimation from biomass burning (Huo et al., 2021). Phenols only account for

265   11.0% of SOA estimation in this work. Alcohols (7.3%) and furans (7.6%) are much more important

266   SOA precursors in incense burning compared to biomass burning and cooking emissions. Compared

267   with other sources, we stress the importance of incense-burning benzenes, furfural, alcohols, and

268   phenols in OFP formation and alcohols and furans in SOA formation. The secondary formation

269   potential of mosquito coils is the lowest, while OFP and SOA of burning smokeless sandalwood

270   sticks are the highest. Compared to other incense, the higher aromatic contents of smokeless

271 sandalwood sticks burning fumes result in much more ozone and SOA formation.

3.3 Identification of molecular markers from incense burning

273 Pixel-based MPCA is utilized to identify tracers of incense burning emissions. In brief, MPCA

274 decomposes a matrix X into a scoring matrix (S) and a loading matrix (L). Similarities and

275 differences in chromatograms are revealed by positive and negative loadings, respectively (Figure 2)

276 (Song et al., 2022b). The similarities of chromatograms could be explained by benzenes (toluene,

277 *p*-xylene, *o*-xylene, and ethylbenzene), ketones (3-methyl-2-cyclopenten-1-one,

278 2-hydroxy-2-cyclopenten-1-one, 3-ethyl-2-pentanone), aldehydes (furfural, succindialdehyde,

279 2-methyl-2-butenal), 2-methyl-propanoic acid, 1-methyl-1H-pyrazole, 2(5H)-furanone, and

280 2-furanmethanol. The differences between samples could be largely explained by 2-methyl-2-butenal,

281 2(5H)-furanone, 3,4-dimethylfuran, 2,3-dihydro-1H-inden-1-one, 2-methoxy-naphthalene, and

282 1,2-dihydro-2,2,4-trimethyl-quinoline. The negative loadings (0.006) are significantly smaller than

283 the positive loadings (0.07), confirming the dominance of similarities among chromatograms. The

284 relationship between the EFs of these compounds among different incense types is displayed in

285 Figure S13. Although the total EFs are significantly different ($p = 0.03$), the EFs of selected

286 compounds (2-hydroxy-2-cyclopenten-1-one, 2-furanmethanol, 3-ethyl-2-pentanone, and furfural are

287 significantly no different ($p > 0.08$). As a result, we recommend these compounds as incense-burning

288 tracers. It is reported that furfural is formed during the thermal degradation of hemicelluloses (Uhde

289 and Salthammer, 2007), while the oxidation of furfural under harsher conditions forms

290 2(5H)-furanone (Depoorter et al., 2021). The formation mechanism of furfural from xylose and

291 D-xylopyranose is displayed in Figure S14 (Ahmad et al., 1995; Bonner and Roth1, 1959; Nimlos et

292 al., 2006). The initiation of the degradation of five-carbon sugars is from the acyclic form of pentoses

293 or directly via a 2,3-(α,β-)unsaturated aldehyde. The dehydrating of the intermediate compounds

294 finally forms furfural (Figure S14). The addressed tracers, furfural, 2-furanmethanol, and

295 2(5H)-furanone, have already been identified in incense burning smoke in previous work (Depoorter

296 et al., 2021; Tran and Marriott, 2007).

297 Furthermore, we compare the chemical profiles with an odor database (Aroma Office 2D,

298 Gerstel). Among the top 20 chemicals contributing to EFs, furfural (bread-like, alcoholic,

incense-like), phenol (mushroom, acid, burnt plastics), 1-hydroxy-2-propanone (buttery, caramellic, fruity), benzyl alcohol (burning taste, flower, roasted), limonene (citrus-like, fruity, lemon-like), and 2-methyl-propanoic acid (apple-like, cheese-like, sweat) could be the aroma compounds. As for tracers identified above, 2-furanmethanol (burnt sugar, honey, sweet) could also be another aroma compound. Among them, furfural is widely and largely detected which could be the most important molecular marker of incense burning (Silva et al., 2021; Ho and Yu, 2002). Note that aromandendrene, a cucumber-like, woody, and floral compound, is only detected in one incense coil sample (incense coil 2, Figure S1). Aromandendrene is also detected in plants, such as in dry flowers of *Lonicera japonica* (Shang et al., 2011). The emission factor of aromandendrene is rather large (4.3 μg g^{-1}, 0.7% of the total EFs), and is a significant SOA precursor (2.3 μg g^{-1}, 3.9% of the total SOA estimation). The importance of aromandendrene on incense flavor and SOA formation could not be neglected. Aromandendrene could also be responsible for the distinct flavor of a certain incense coil. As above said, we recommend furfural be used as a molecular indicator of incense burning regardless of the incense type or additives, especially responsible for the flavor of incense burning.

3.4   Risk assessment of incense burning organics

The hazardous compounds from incense burning could cause adverse health effects on human health (Wong et al., 2020; Yang et al., 2007; Chen et al., 2021; Yang et al., 2017). To evaluate the potential risks of these compounds, we conducted a pixel-based risk assessment (bioaccumulation potential, BAP) for partition coefficient estimation. Chemicals with high BAP concerns are listed in Figure 3. 2-methoxy-naphthalene, acenaphthylene, dibenzofuran, diethyl phthalate, dibutyl phthalate, benzoic acid 2-ethylhexyl ester, C15 – C19 *n,* and *b*-alkanes are regarded as high BAP concern (Figure 3). Among them, acenaphthylene is a toxic polycyclic aromatic hydrocarbon (PAH) that is widely detected in incense smoke (Yadav et al., 2022). Dibenzofuran, an oxygenated compound with detrimental effects on human health (Suzuki et al., 2021), is also detected in the smoke of incense burning (Tran and Marriott, 2007). Diethyl phthalate and dibutyl phthalate are phthalate esters (PAEs) widely used as plasticizers which are endocrine disruptors (Wang and Qian, 2021). PAEs are abundant in incense smoke (Tran and Marriott, 2007). We propose that acenaphthylene, dibenzofuran, and PAEs could be chemicals of high-risk concern in incense smoke. We also assess the arctic

327 contamination potential (ACP) as shown in Text S1. Further epidemiologic studies should be carried

328 on to demonstrate the health effect of these hazardous compounds.

4 Implication

330 The non-target approach of GC×GC-MS gives us a full glimpse of incense smoke, spotting a

331 large pool of organics (317 compounds) covering the VOC-IVOC-SVOC range. We have provided a

332 detailed description of both primary emission and secondary estimation of incense burning organics

333 which is ready-to-use in SOA simulation models. IVOCs (130 compounds) are crucial organics

334 accounting for 19.2% of the total EFs and 40.0% of the SOA estimation, highlighting the importance

335 of incorporating IVOCs into SOA models. Further investigation should be carried on to elucidate

336 emission characteristics of short-chain compounds that are lacking in our research, such as alkanes

337 (<C7), alkenes (<C7), and aldehydes (<C5). By combining data obtained from

338 gas-chromatography-flame ionization detector (GC-FID) and proton transfer mass spectrometer

339 (PTR-MS), the emission pattern of incense burning could be well demonstrated. Comparisons of

340 IVOC capture efficiency on different sampling materials should also be taken into account to obtain

341 a reliable quantification result of IVOC species. High-time resolution measurement should also be

342 carried on to understand the time-resolved pattern of incense burning.

343 We also suggest furfural as the molecular marker of incense burning as the EFs of furfural

344 among samples are relatively stable. Pixel-based MPCA also indicates that furfural is responsible for

345 the similarities between chromatograms. Furfural may be the key aroma compound of incense smoke.

346 This key component identified in this work could be implemented in source apportionment. Furfural

347 is also a key component contributing to OFP (rank 2). Phenol, toluene, 2-furanmethanol, benzene,

348 and benzyl alcohol are the main contributors to both OFP and SOA.

349 Surprisingly, we find that the EF of burning smokeless sandalwood sticks is the highest, with a

350 remarkable contribution to OFP and SOA, due to the high aromatic contents. We recommend that

351 both gaseous and particulate organics should also be taken into consideration when burning incense.

352 The single reduction of particles does not mean fewer emissions of gas-phase organics. A

353 comprehensive assessment of incense-burning organics in both gas- and particle-phase should be

354 implemented.

355   Combing pixel-based property estimation and blob identification, the risk assessment analysis of

356   compounds could benefit analysts with less experience with GC×GC. The risk assessment in this

357   work demonstrates that acenaphthylene, dibenzofuran, and PAEs are chemicals of high-risk concern

358   and warrant further control. It was reported that more than half of Chinese residents burn incense

359   every day at home for more than 20 years (Salvi and Apte, 2016). The toxic PAHs detected in indoor

360   air could be 19 times higher than in outdoor air (Salvi and Apte, 2016). Exposure to these hazardous

361   compounds could result in significant health threats. As a result, it is of vital importance to reveal

362   and assess the epidemiological influences of incense burning in future work.

363

Reference

Ahmad, T., Kenne, L., Olsson, K., and Theander, O.: The formation of 2-furaldehyde and formic acid from pentoses in slightly acidic deuterium oxide studied by 1H NMR spectroscopy, Carbohydr Res, 276, 309–320, https://doi.org/10.1016/0008-6215(95)00176-T, 1995.

Alam, M. S., Zeraati-Rezaei, S., Liang, Z., Stark, C., Xu, H., MacKenzie, A. R., and Harrison, R. M.: Mapping and quantifying isomer sets of hydrocarbons (≥C12) in diesel exhaust, lubricating oil and diesel fuel samples using GC× GC-ToF-MS, Atmos Meas Tech, 11, 3047–3058, https://doi.org/10.5194/amt-11-3047-2018, 2018.

Algrim, L. B. and Ziemann, P. J.: Effect of the Keto Group on Yields and Composition of Organic Aerosol Formed from OH Radical-Initiated Reactions of Ketones in the Presence of NOx, Journal of Physical Chemistry A, 120, 6978–6989, https://doi.org/10.1021/acs.jpca.6b05839, 2016.

Algrim, L. B. and Ziemann, P. J.: Effect of the Hydroxyl Group on Yields and Composition of Organic Aerosol Formed from OH Radical-Initiated Reactions of Alcohols in the Presence of NOx, ACS Earth Space Chem, 3, 413–423, https://doi.org/10.1021/acsearthspacechem.9b00015, 2019.

Bonner, W. A. and Roth1, M. R.: The Conversion of d-Xylose-l-C14 into 2-Furaldehyde-α-C14, J Am Chem Soc, 81, 5454–5456, https://doi.org/10.1021/ja01529a051, 1959.

Chan, A. W. H., Kautzman, K. E., Chhabra, P. S., Surratt, J. D., Chan, M. N., Crounse, J. D., Kürten, A., Wennberg, P. O., Flagan, R. C., and Seinfeld, J. H.: Secondary organic aerosol formation from photooxidation of naphthalene and alkylnaphthalenes: Implications for oxidation of intermediate volatility organic compounds (IVOCs), Atmos Chem Phys, 9, 3049–3060, https://doi.org/10.5194/acp-9-3049-2009, 2009.

Chan, A. W. H., Chan, M. N., Surratt, J. D., Chhabra, P. S., Loza, C. L., Crounse, J. D., Yee, L. D., Flagan, R. C., Wennberg, P. O., and Seinfeld, J. H.: Role of aldehyde chemistry and NOx concentrations in secondary organic aerosol formation, Atmos Chem Phys, 10, 7169–7188, https://doi.org/10.5194/ACP-10-7169-2010, 2010.

Charan, S. M., Buenconsejo, R. S., and Seinfeld, J. H.: Secondary organic aerosol yields from the oxidation of benzyl alcohol, Atmos Chem Phys, 20, 13167–13190, https://doi.org/10.5194/acp-20-13167-2020, 2020.

398 Chen, K. S. F., Tsai, Y. P., Lai, C. H., Xiang, Y. K., Chuang, K. Y., and Zhu, Z. H.: Human health-risk

399 assessment based on chronic exposure to the carbonyl compounds and metals emitted by burning

400 incense at temples, Environmental Science and Pollution Research, 28, 40640–40652,

401 https://doi.org/10.1007/s11356-020-10313-1, 2021.

402 Depoorter, A., Kalalian, C., Emmelin, C., Lorentz, C., and George, C.: Indoor heterogeneous

403 photochemistry of furfural drives emissions of nitrous acid, Indoor Air, 31, 682–692,

404 https://doi.org/10.1111/INA.12758, 2021.

405 Drozd, G. T., Zhao, Y., Saliba, G., Frodin, B., Maddox, C., Oliver Chang, M. C., Maldonado, H.,

406 Sardar, S., Weber, R. J., Robinson, A. L., Goldstein, A. H., Chang, M. C. O., Maldonado, H., Sarder, S.,

407 Weber, R. J., Robinson, A. L., Goldstein, A. H., Oliver Chang, M. C., Maldonado, H., Sardar, S.,

408 Weber, R. J., Robinson, A. L., and Goldstein, A. H.: Detailed Speciation of Intermediate Volatility and

409 Semivolatile Organic Compound Emissions from Gasoline Vehicles: Effects of Cold-Starts and

410 Implications for Secondary Organic Aerosol Formation, Environ Sci Technol, 53, 1706–1714,

411 https://doi.org/10.1021/acs.est.8b05600, 2019.

412 Guo, S., Hu, M., Zamora, M. L., Peng, J., Shang, D., Zheng, J., Du, Z., Wu, Z., Shao, M., Zeng, L.,

413 Molina, M. J., and Zhang, R.: Elucidating severe urban haze formation in China, Proc Natl Acad Sci U

414 S A, 111, 17373–17378, https://doi.org/10.1073/pnas.1419604111, 2014.

415 Guo, S., Hu, M., Peng, J., Wu, Z., Zamora, M. L., Shang, D., Du, Z., Zheng, J., Fang, X., Tang, R., Wu,

416 Y., Zeng, L., Shuai, S., Zhang, W., Wang, Y., Ji, Y., Li, Y., Zhang, A. L., Wang, W., Zhang, F., Zhao, J.,

417 Gong, X., Wang, C., Molina, M. J., and Zhang, R.: Remarkable nucleation and growth of ultrafine

418 particles from vehicular exhaust, Proc Natl Acad Sci U S A, 117, 3427–3432,

419 https://doi.org/10.1073/pnas.1916366117, 2020.

420 Harvey, R. M. and Petrucci, G. A.: Control of ozonolysis kinetics and aerosol yield by nuances in the

421 molecular structure of volatile organic compounds, Atmos Environ, 122, 188–195,

422 https://doi.org/10.1016/j.atmosenv.2015.09.038, 2015.

423 He, X., Zheng, X., You, Y., Zhang, S., Zhao, B., Wang, X., Huang, G., Chen, T., Cao, Y., He, L., Chang,

424 X., Wang, S., and Wu, Y.: Comprehensive chemical characterization of gaseous I/SVOC emissions

425 from heavy-duty diesel vehicles using two-dimensional gas chromatography time-of-flight mass

spectrometry, Environmental Pollution, 305, 119284, https://doi.org/10.1016/j.envpol.2022.119284, 2022.

Ho, S. S. H. and Yu, J. Z.: Concentrations of formaldehyde and other carbonyls in environments affected by incense burning, Journal of Environmental Monitoring, 4, 728–733, https://doi.org/10.1039/b200998f, 2002.

Huo, Y., Guo, Z., Liu, Y., Wu, D., Ding, X., Zhao, Z., Wu, M., Wang, L., Feng, Y., Chen, Y., Wang, S., Li, Q., and Chen, J.: Addressing Unresolved Complex Mixture of I/SVOCs Emitted From Incomplete Combustion of Solid Fuels by Nontarget Analysis, Journal of Geophysical Research: Atmospheres, 126, e2021JD035835, https://doi.org/10.1029/2021JD035835, 2021.

Jetter, J. J., Guo, Z., McBrian, J. A., and Flynn, M. R.: Characterization of emissions from burning incense, Science of the Total Environment, 295, 51–67, https://doi.org/10.1016/S0048-9697(02)00043-8, 2002.

Lee, S. C. and Wang, B.: Characteristics of emissions of air pollutants from burning of incense in a large environmental chamber, Atmos Environ, 38, 941–951, https://doi.org/10.1016/j.atmosenv.2003.11.002, 2004.

Li, L., Tang, P., Nakao, S., and Cocker, D. R.: Impact of molecular structure on secondary organic aerosol formation from aromatic hydrocarbon photooxidation under low-NOx conditions, Atmos Chem Phys, 16, 10793–10808, https://doi.org/10.5194/acp-16-10793-2016, 2016.

Liu, T., Wang, Z., Huang, D. D., Wang, X., and Chan, C. K.: Significant Production of Secondary Organic Aerosol from Emissions of Heated Cooking Oils, Environ Sci Technol Lett, 5, 32–37, https://doi.org/10.1021/acs.estlett.7b00530, 2018.

Loza, C. L., Craven, J. S., Yee, L. D., Coggon, M. M., Schwantes, R. H., Shiraiwa, M., Zhang, X., Schilling, K. A., Ng, N. L., Canagaratna, M. R., Ziemann, P. J., Flagan, R. C., and Seinfeld, J. H.: Secondary organic aerosol yields of 12-carbon alkanes, Atmos Chem Phys, 14, 1423–1439, https://doi.org/10.5194/acp-14-1423-2014, 2014.

Lu, F., Li, S., Shen, B., Zhang, J., Liu, L., Shen, X., and Zhao, R.: The emission characteristic of VOCs and the toxicity of BTEX from different mosquito-repellent incenses, J Hazard Mater, 384, 121428, https://doi.org/10.1016/j.jhazmat.2019.121428, 2020.

454   Lu, Q., Zhao, Y., and Robinson, A. L.: Comprehensive organic emission profiles for gasoline, diesel,

455   and gas-turbine engines including intermediate and semi-volatile organic compound emissions, Atmos

456   Chem Phys, 18, 17637–17654, https://doi.org/10.5194/acp-18-17637-2018, 2018.

457   Manoukian, A., Quivet, E., Temime-Roussel, B., Nicolas, M., Maupetit, F., and Wortham, H.:

458   Emission characteristics of air pollutants from incense and candle burning in indoor atmospheres,

459   Environmental   Science   and   Pollution   Research,   20,   4659–4670,

460   https://doi.org/10.1007/s11356-012-1394-y, 2013.

461   Manoukian, A., Buiron, D., Temime-Roussel, B., Wortham, H., and Quivet, E.: Measurements of

462   VOC/SVOC emission factors from burning incenses in an environmental test chamber: influence of

463   temperature, relative humidity, and air exchange rate, Environmental Science and Pollution Research,

464   23, 6300–6311, https://doi.org/10.1007/s11356-015-5819-2, 2016.

465   Matsunaga, A., Docherty, K. S., Lim, Y. B., and Ziemann, P. J.: Composition and yields of secondary

466   organic aerosol formed from OH radical-initiated reactions of linear alkenes in the presence of NOx:

467   Modeling   and   measurements,   Atmos   Environ,   43,   1349–1357,

468   https://doi.org/10.1016/j.atmosenv.2008.12.004, 2009.

469   McDonald, B. C., De Gouw, J. A., Gilman, J. B., Jathar, S. H., Akherati, A., Cappa, C. D., Jimenez, J.

470   L., Lee-Taylor, J., Hayes, P. L., McKeen, S. A., Cui, Y. Y., Kim, S. W., Gentner, D. R.,

471   Isaacman-VanWertz, G., Goldstein, A. H., Harley, R. A., Frost, G. J., Roberts, J. M., Ryerson, T. B.,

472   and Trainer, M.: Volatile chemical products emerging as largest petrochemical source of urban organic

473   emissions, Science (1979), 359, 760–764, https://doi.org/10.1126/science.aaq0524, 2018.

474   Nabi, D., Gros, J., Dimitriou-Christidis, P., and Arey, J. S.: Mapping environmental partitioning

475   properties of nonpolar complex mixtures by use of GC × GC, Environ Sci Technol, 48, 6814–6826,

476   https://doi.org/10.1021/es501674p, 2014.

477   Nimlos, M. R., Qian, X., Davis, M., Himmel, M. E., and Johnson, D. K.: Energetics of xylose

478   decomposition as determined using quantum mechanics modeling, Journal of Physical Chemistry A,

479   110, 11824–11838, https://doi.org/10.1021/jp0626770, 2006.

480   Salvi, S. and Apte, K.: Household air pollution and its effects on health, F1000Res, 5,

481   https://doi.org/10.12688/f1000research.7552.1, 2016.

482　Shah, R. U., Coggon, M. M., Gkatzelis, G. I., McDonald, B. C., Tasoglou, A., Huber, H., Gilman, J.,

483　Warneke, C., Robinson, A. L., and Presto, A. A.: Urban Oxidation Flow Reactor Measurements Reveal

484　Significant Secondary Organic Aerosol Contributions from Volatile Emissions of Emerging

485　Importance, Environ Sci Technol, 54, 714–725, https://doi.org/10.1021/acs.est.9b06531, 2020.

486　Shang, X., Pan, H., Li, M., Miao, X., and Ding, H.: Lonicera japonica Thunb.: Ethnopharmacology,

487　phytochemistry and pharmacology of an important traditional Chinese medicine,

488　https://doi.org/10.1016/j.jep.2011.08.016, 2011.

489　Silva, G. V., Martins, A. O., and Martins, S. D. S.: Indoor air quality: Assessment of dangerous

490　substances in incense products, Int J Environ Res Public Health, 18,

491　https://doi.org/10.3390/ijerph18158086, 2021.

492　Song, K., Guo, S., Gong, Y., Lv, D., Zhang, Y., Wan, Z., Li, T., Zhu, W., Wang, H., Yu, Y., Tan, R.,

493　Shen, R., Lu, S., Li, S., Chen, Y., and Hu, M.: Impact of cooking style and oil on semi-volatile and

494　intermediate volatility organic compound emissions from Chinese domestic cooking, Atmos Chem

495　Phys, 22, 9827–9841, https://doi.org/10.5194/ACP-22-9827-2022, 2022a.

496　Song, K., Gong, Y., Guo, S., Lv, D., Wang, H., Wan, Z., Yu, Y., Tang, R., Li, T., Tan, R., Zhu, W., Shen,

497　R., and Lu, S.: Investigation of partition coefficients and fingerprints of atmospheric gas- and

498　particle-phase intermediate volatility and semi-volatile organic compounds using pixel-based

499　approaches, J Chromatogr A, 1665, 462808, https://doi.org/10.1016/j.chroma.2022.462808, 2022b.

500　Song, K., Guo, S., Gong, Y., Lv, D., Wan, Z., Zhang, Y., Fu, Z., Hu, K., and Lu, S.: Non-target scanning

501　of organics from cooking emissions using comprehensive two-dimensional gas chromatography-mass

502　spectrometer (GC×GC-MS), Applied Geochemistry, 151,

503　https://doi.org/10.1016/j.apgeochem.2023.105601, 2023.

504　Staub, P. O., Schiestl, F. P., Leonti, M., and Weckerle, C. S.: Chemical analysis of incense smokes used

505　in Shaxi, Southwest China: A novel methodological approach in ethnobotany, J Ethnopharmacol, 138,

506　212–218, https://doi.org/10.1016/j.jep.2011.08.078, 2011.

507　Stewart, G. J., Nelson, B. S., Acton, W. J. F., Vaughan, A. R., Hopkins, J. R., Yunus, S. S. M., Hewitt, C.

508　N., Nemitz, E., Mandal, T. K., Gadi, R., Sahu, Lokesh. K., Rickard, A. R., Lee, J. D., and Hamilton, J.

509　F.: Comprehensive organic emission profiles, secondary organic aerosol production potential, and OH

reactivity of domestic fuel combustion in Delhi, India, Environmental Science: Atmospheres, 1, 104–117, https://doi.org/10.1039/d0ea00009d, 2021.

Suzuki, S., Kiuchi, S., Kinoshita, K., Takeda, Y., Sakaida, S., Konno, M., Tanaka, K., and Oguma, M.: Formation of polycyclic aromatic hydrocarbons, benzofuran, and dibenzofuran in fuel-rich oxidation of toluene using a flow reactor, Physical Chemistry Chemical Physics, 23, 6509–6525, https://doi.org/10.1039/d0cp06615j, 2021.

Tang, R., Lu, Q., Guo, S., Wang, H., Song, K., Yu, Y., Tan, R., Liu, K., Shen, R., Chen, S., Zeng, L., Jorga, S. D., Zhang, Z., Zhang, W., Shuai, S., and Robinson, A. L.: Measurement report: Distinct emissions and volatility distribution of intermediate-volatility organic compounds from on-road Chinese gasoline vehicles: Implication of high secondary organic aerosol formation potential, Atmos Chem Phys, 21, 2569–2583, https://doi.org/10.5194/acp-21-2569-2021, 2021.

Tkacik, D. S., Presto, A. A., Donahue, N. M., and Robinson, A. L.: Secondary organic aerosol formation from intermediate-volatility organic compounds: Cyclic, linear, and branched alkanes, Environ Sci Technol, 46, 8773–8781, https://doi.org/10.1021/es301112c, 2012.

Tran, T. C. and Marriott, P. J.: Characterization of incense smoke by solid phase microextraction-Comprehensive two-dimensional gas chromatography (GC×GC), Atmos Environ, 41, 5756–5768, https://doi.org/10.1016/j.atmosenv.2007.02.030, 2007.

Uhde, E. and Salthammer, T.: Impact of reaction products from building materials and furnishings on indoor air quality-A review of recent advances in indoor chemistry, Atmos Environ, 41, 3111–3128, https://doi.org/10.1016/j.atmosenv.2006.05.082, 2007.

Wang, J., Jin, L., Gao, J., Shi, J., Zhao, Y., Liu, S., Jin, T., Bai, Z., and Wu, C. Y.: Investigation of speciated VOC in gasoline vehicular exhaust under ECE and EUDC test cycles, Science of the Total Environment, 445–446, 110–116, https://doi.org/10.1016/j.scitotenv.2012.12.044, 2013.

Wang, Y. and Qian, H.: Phthalates and their impacts on human health, https://doi.org/10.3390/healthcare9050603, 2021.

Wong, A., Lou, W., Ho, K. fai K., Yiu, B. K. fung, Lin, S., Chu, W. C. wing, Abrigo, J., Lee, D., Lam, B. Y. ka, Au, L. W. chi, Soo, Y. O. yan, Lau, A. Y. lun, Kwok, T. C. yui, Leung, T. W. hong, Lam, L. C. wa, Ho, K. fai K., and Mok, V. C. tong: Indoor incense burning impacts cognitive functions and brain

538 functional connectivity in community older adults, Sci Rep, 10, 1–11,

539 https://doi.org/10.1038/s41598-020-63568-6, 2020.

540 Wu, W., Zhao, B., Wang, S., and Hao, J.: Ozone and secondary organic aerosol formation potential

541 from anthropogenic volatile organic compounds emissions in China, J Environ Sci (China), 53, 224–

542 237, https://doi.org/10.1016/j.jes.2016.03.025, 2017.

543 Yadav, V. K., Malik, P., Tirth, V., Khan, S. H., Yadav, K. K., Islam, S., Choudhary, N., Inwati, G. K.,

544 Arabi, A., Kim, D. H., and Jeon, B. H.: Health and Environmental Risks of Incense Smoke:

545 Mechanistic Insights and Cumulative Evidence, J Inflamm Res, 15, 2665–2693,

546 https://doi.org/10.2147/JIR.S347489, 2022.

547 Yang, T. T., Lin, T. S., and Chang, M.: Characteristics of emissions of volatile organic compounds

548 from smoldering incense, Bull Environ Contam Toxicol, 78, 308–313,

549 https://doi.org/10.1007/s00128-007-9184-9, 2007.

550 Yang, T. T., Ho, S. C., Chuang, L. te, Chuang, H. C., Li, Y. T., and Wu, J. J.: Characterization of

551 particulate-phase polycyclic aromatic hydrocarbons emitted from incense burning and their

552 bioreactivity in RAW264.7 macrophage, Environmental Pollution, 220, 1190–1198,

553 https://doi.org/10.1016/j.envpol.2016.11.016, 2017.

554 Yu, Y., Guo, S., Wang, H., Shen, R., Zhu, W., Tan, R., Song, K., Zhang, Z., Li, S., Chen, Y., and Hu, M.:

555 Importance of Semivolatile/Intermediate-Volatility Organic Compounds to Secondary Organic

556 Aerosol Formation from Chinese Domestic Cooking Emissions, Environ Sci Technol Lett,

557 https://doi.org/10.1021/acs.estlett.2c00207, 2022.

558 Yue, T., Yue, X., Chai, F., Hu, J., Lai, Y., He, L., and Zhu, R.: Characteristics of volatile organic

559 compounds (VOCs) from the evaporative emissions of modern passenger cars, Atmos Environ, 151,

560 62–69, https://doi.org/10.1016/j.atmosenv.2016.12.008, 2017.

561 Zhao, Y., Hu, M., Slanina, S., and Zhang, Y.: Chemical compositions of fine particulate organic matter

562 emitted from Chinese cooking, Environ Sci Technol, 41, 99–105, https://doi.org/10.1021/es0614518,

563 2007.

564 Zhao, Y., Hennigan, C. J., May, A. A., Tkacik, D. S., de Gouw, J. A., Gilman, J. B., Kuster, W. C.,

565 Borbon, A., and Robinson, A. L.: Intermediate-volatility organic compounds: A large source of

566 secondary organic aerosol, Environ Sci Technol, 48, 13743–13750, https://doi.org/10.1021/es5035188,

567 2014.

568 Zhao, Y., Nguyen, N. T., Presto, A. A., Hennigan, C. J., May, A. A., and Robinson, A. L.: Intermediate

569 Volatility Organic Compound Emissions from On-Road Diesel Vehicles: Chemical Composition,

570 Emission Factors, and Estimated Secondary Organic Aerosol Production, Environ Sci Technol, 49,

571 11516–11526, https://doi.org/10.1021/acs.est.5b02841, 2015.

572 Zhao, Y., Saleh, R., Saliba, G., Presto, A. A., Gordon, T. D., Drozd, G. T., Goldstein, A. H., Donahue,

573 N. M., and Robinson, A. L.: Reducing secondary organic aerosol formation from gasoline vehicle

574 exhaust, Proc Natl Acad Sci U S A, 114, 6984–6989, https://doi.org/10.1073/pnas.1620911114, 2017.

575 Zhu, X., Han, Y., Feng, Y., Cheng, P., Peng, Y., Wang, J., Cai, J., and Chen, Y.: Formation and emission

576 characteristics of intermediate volatile organic compounds (IVOCs) from the combustion of biomass

577 and their cellulose, hemicellulose, and lignin, Atmos Environ, 286, 119217,

578 https://doi.org/10.1016/j.atmosenv.2022.119217, 2022.

579 Zushi, Y., Yamatori, Y., Nagata, J., and Nabi, D.: Comprehensive two-dimensional

580 gas-chromatography-based property estimation to assess the fate and behavior of complex mixtures: A

581 case study of vehicle engine oil, Science of the Total Environment, 669, 739–745,

582 https://doi.org/10.1016/j.scitotenv.2019.03.157, 2019.

583

584 **Figures**

585 **Figure 1.** Volatility distributions of EF, OFP, and SOA with chemical class in each volatility bin. The

586 *x*-axis is the unsaturated vapor concentration in logarithmic form (log C*, μg m^{-3}). The *y*-axis is the
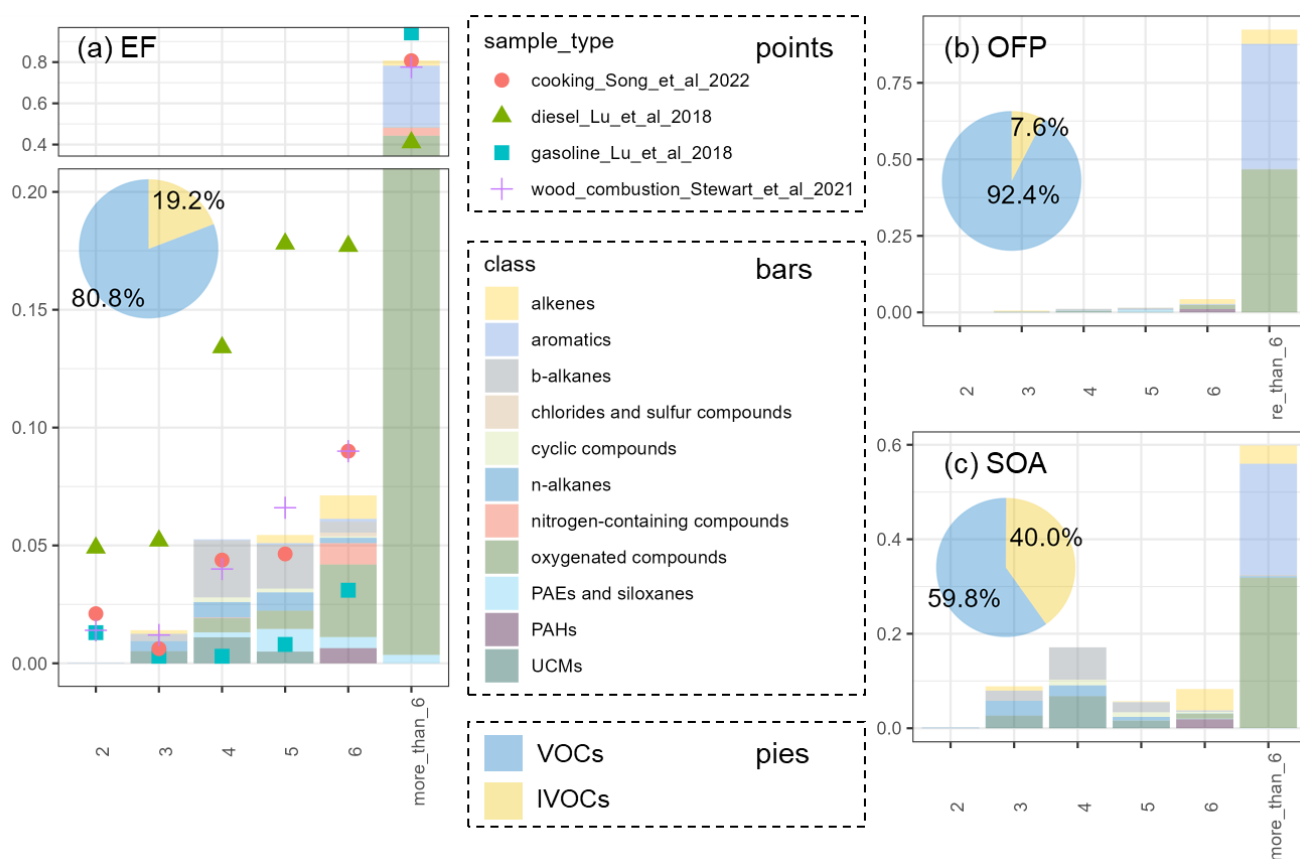
587 normalized mass emission factor (100%).

588 **Figure 2.** Positive (a) and negative loadings (b) of incense burning samples describing similarities

589 and differences between chromatograms. The color bar is the loading.

590 **Figure 3.** Chemicals with high bioaccumulation potential (BAP) assesses by pixel-based approaches.
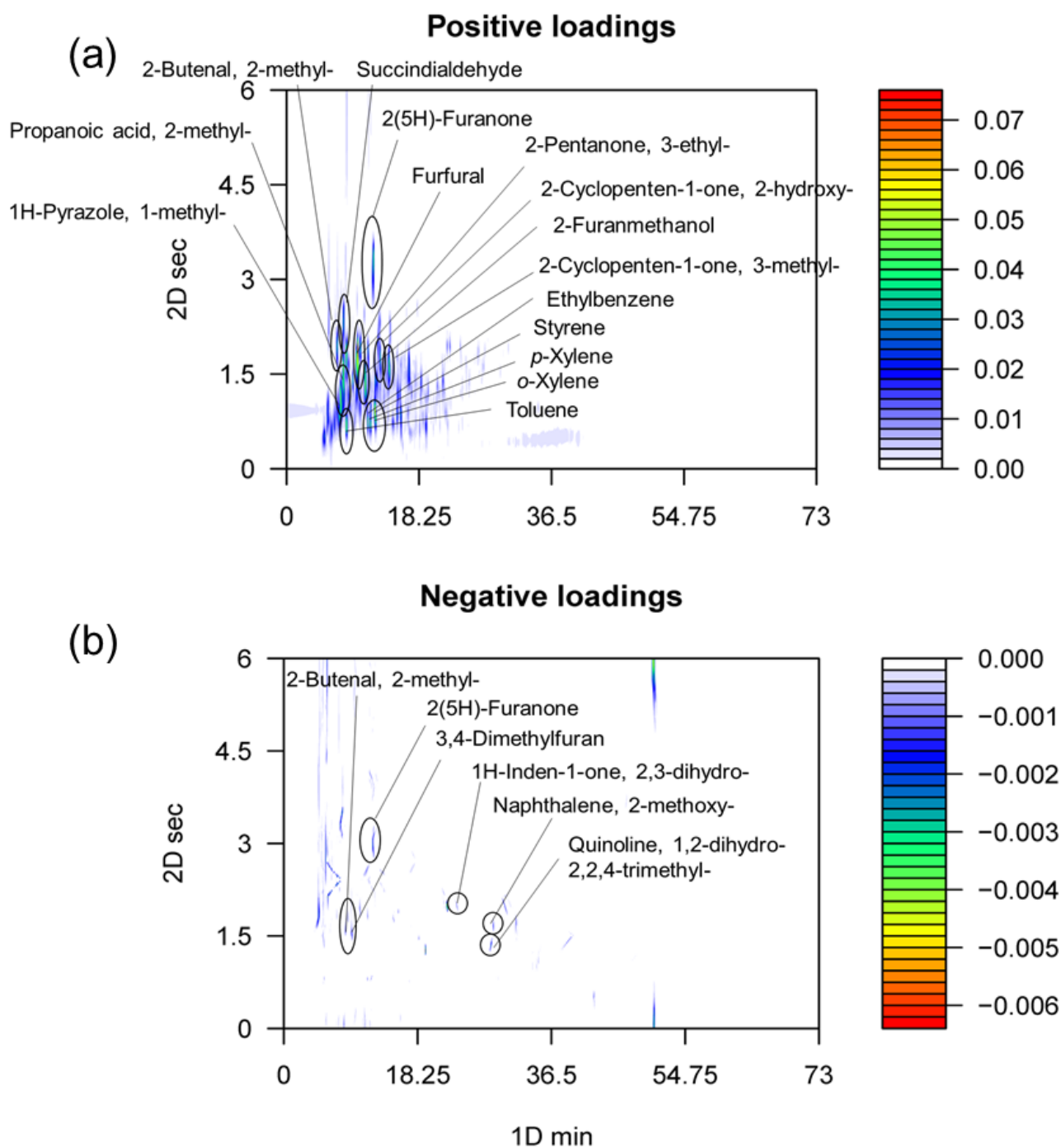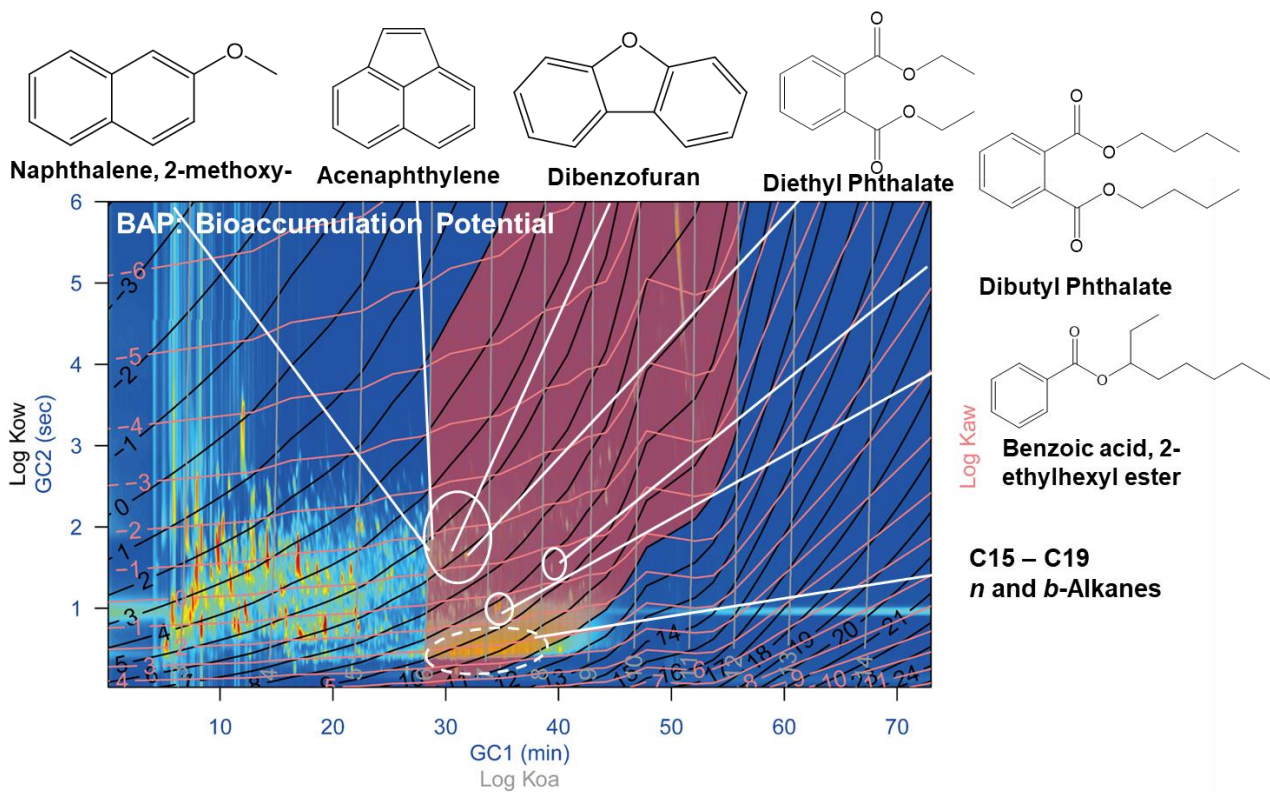
591

592

593

594

595

596 **Figure 1.** Volatility distributions of EF, OFP, and SOA with chemical class in each volatility bin. The

597 x-axis is the unsaturated vapor concentration in logarithmic form (log C*, μg m^{-3}). The y-axis is the

598 normalized mass emission factor (100%).

Figure 2. Positive (a) and negative loadings (b) of incense burning samples describing similarities and differences between chromatograms. The color bar is the loading.

Figure 3. Chemicals with high bioaccumulation potential (BAP) assesses by pixel-based approaches.